

Robust intrinsic ferromagnetism in 2D half-metallic material MnAsS₄Tengfei Hu,¹ Wenhui Wan,¹ Yanfeng Ge,¹ and Yong Liu^{1, a)}

State Key Laboratory of Metastable Materials Science and Technology & Key Laboratory for Microstructural Material Physics of Hebei Province, School of Science, Yanshan University, Qinhuangdao 066004, China

Two-dimensional (2D) intrinsic half-metallic materials are of great interest to explore the exciting physics and applications of nanoscale spintronic devices, but no such materials have been experimentally realized. Using first-principles calculations based on density-functional theory (DFT), we predicted that single-layer MnAsS₄ was a 2D intrinsic ferromagnetic (FM) half-metal. The half-metallic spin gap for single-layer MnAsS₄ is about 1.46 eV, and it has a large spin splitting of about 0.49 eV in the conduction band. Monte Carlo simulations predicted the Curie temperature (T_c) was about 740 K. Moreover, Within the biaxial strain ranging from -5% to 5%, the FM half-metallic properties remain unchanged. Its ground-state with 100% spin-polarization ratio at Fermi level may be a promising candidate material for 2D spintronic applications.

^{a)}Electronic mail: yongliu@ysu.edu.cn, or ycliu@ysu.edu.cn

I. INTRODUCTION

Spintronics, which uses the spin of electrons for the information storage, transport and processing, have attracted intensive interests from the viewpoint of fundamental science and technology applications in the past decades¹. It is important in the field of quantum computing and the next-generation information technology^{2,3}. Half-metallic materials, which is conducting in one spin orientation but insulating in the opposite spin direction meet the demand of a 100% spin polarization ratio, are highly desirable for advanced spintronic applications⁴. The band gap for the insulating channel is termed as spin gap. To prevent spin leakage, the spin gap needs to be as wide as possible⁵. Since the first half-metallic material NiMnSb was predicted in 1983⁶, there has been a flurry of research into magnetic half-metals, such as transition metal compounds MnX (X = P, As), NbF₃, CoH₂, ScH₂, TiCl₃, VCl₃⁷⁻¹⁰; sp half-metallic ferromagnets RbSe and CsTe¹¹⁻¹⁴.

Although half-metallic material has been studied for a long time, the demonstrated half-metals was very limited and have serious shortcomings, such as high cost or low T_c . Until now, intrinsic half-metallic material with wide spin gap and high T_c is still absent in experiments. However, the single-layer CrPS₄¹⁵ was predicted to be a ferromagnetic semiconductor and the valance bands are splited for different spin orientation. As hole doping can lower Fermi level into the valence bands of one spin and lead to half-metallic ferromagnets. An obvious option is to replace Cr by Mn atoms, and by stability calculation we replace P with As atoms.

In this paper, the first-principles calculations are used to investigate the mechanical, dynamical, electronic and magnetic properties of single-layer MnAsS₄. Our calculations indicate that the MnAsS₄ crystal is mechanically and dynamically stable, so it is possibly prepared. It is metallic at the Fermi level in one spin direction and has a band gap of 1.46 eV in the opposite spin direction. Its half-metallic properties do not change under the biaxial strain range from -5% to 5%. It has stable ferromagnetism phase with integer magnetic moment of 8 μ_B per primitive cell. Furthermore, we demonstrated that the MnAsS₄ exhibits high T_c about 740 K.

II. METHODS

Kohn-Sham DFT calculations are performed using the projector augmented wave method, as implemented in the plane-wave code VASP^{16–18}. A cutoff energy of 500 eV and a Monkhorst-Pack special k-point mesh¹⁹ of $17 \times 19 \times 1$ for the Brillouin zone integration was found to be sufficient to obtain the convergence. We used a Perdew-Burke-Ernzerhof (PBE) type generalized gradient approximation (GGA) in the exchange-correlation functional²⁰. A conjugate-gradient algorithm was employed for geometry optimization using convergence criteria of 10^{-7} eV for the total energy and 0.005 eV/Å for Hellmann-Feynman force components. We used GGA+U to treat the strong on-site Coulomb interaction²¹. A series of U values were selected, that is, 1.0-6.0 eV for Mn. Whatever U was, it didn't affected the ground-state of MnAsS₄. Thus, the main conclusions were consistent for the different values of U. So we displayed that results with Hubbard U term 5 eV for Mn²² as suggested by Dudarev *et al*²³. The band structures for different U values can be found in Figure S1. Phonon dispersions were calculated by density functional perturbation theory²⁴ by the Phonopy package interfaced to VASP code with $2 \times 2 \times 1$ supercell. We inserted a 15 Å vacuum slab to avoid the interactions between periodic images.

III. RESULTS AND DISCUSSION

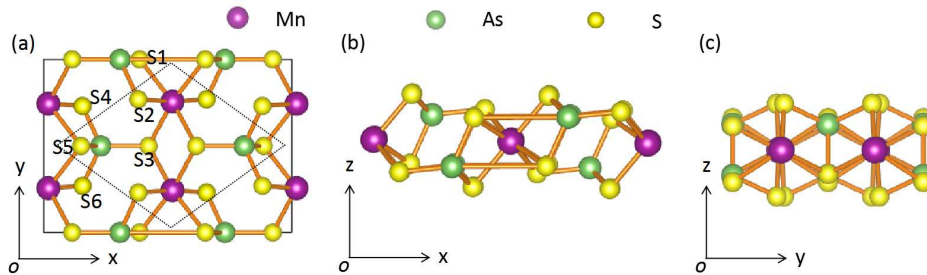


FIG. 1: (Color online) The crystal structure of single-layer MnAsS₄ as seen from the (a) z-direction, (b) y-direction and (c) x-direction. The primitive cell is indicated by dotted line and the unit cell is indicated by solid line in (a).

The atomic structure of single-layer MnAsS₄ is shown in Fig. 1. The unit cell has parameters $a = 11.34$ Å, $b = 7.89$ Å. As shown in Fig. 1 (b), the As atoms bridge the twisted

MnS₆ octahedral chain. A Mn atom connects six S atoms, three types of bond lengths of Mn-S1, Mn-S2, Mn-S3 are 2.635Å, 2.451Å and 2.646Å, respectively. An As atom connects four S atoms and the bond lengths of As-S3, As-S4, As-S5 are 2.198Å, 2.182Å and 2.214Å, respectively, and the As-S6 bond length is the same as As-S4. In the diamond box in Fig. 1 (a) is a primitive cell. A primitive cell contains two Mn atoms. We calculated that each primitive cell is an integer magnetic moment of 8 μ_B , and the local magnetic moment per Mn atom is about 4 μ_B .

To determine the ground-state magnetic order, we compared the total energies of FM and different antiferromagnetic (AFM) structures²⁵. The energy differences ΔE relative to single-layer FM configurations are 170.69, 278.81, and 220.64 meV for the single-layer AFM1, AFM2, and AFM3 configurations, respectively. So the ground-state of single-layer MnAsS₄ is FM. Additionally, the non-magnetic (NM) state can be neglected owing to the great energy disparity between the NM state and magnetic states.

TABLE I: Elastic constants C_{11} , C_{12} and C_{22} (N/m) for single-layer MnAsS₄.

C_{11}	C_{12}	C_{22}
76.69	10.39	71.35

Next, we determined its mechanical stability by calculating the three independent elastic constants. As shown in Table I, we find that $C_{11} = 76.69$ N/m, $C_{12} = 10.39$ N/m and $C_{22} = 71.35$ N/m, respectively. The elastic constants clearly satisfy Borns stability criterion²⁶, i.e., $C_{11} > 0$, $C_{22} > 0$ and $C_{11} - C_{12} > 0$, indicating that they are mechanically stable. Meanwhile, we evaluate the stability of single-layer MnAsS₄ by comparing their binding energies, which is defined as

$$E_b = \frac{2E(Mn) + 2E(As) + 8E(S) - E(MnAsS_4)}{12},$$

where $E(Mn)$, $E(As)$, $E(S)$ and $E(MnAsS_4)$ are the energy of Mn atom, As atom, S atom and single-layer MnAsS₄, respectively. According to this theory, the bigger E_b is, the more stable the system will be. We find the binding energy is 4.03 eV per atom, which is bigger than the synthetic VI₃²⁷ and others^{28,29}.

In order to ensure the single-layer MnAsS₄ is dynamically stable, we calculated its phonon dispersion. As shown in Figure S2, the imaginary frequency is found to be absent in the whole Brillouin zone, it suggests that single-layer MnAsS₄ is dynamically stable and can

exist as free-standing 2D crystal.

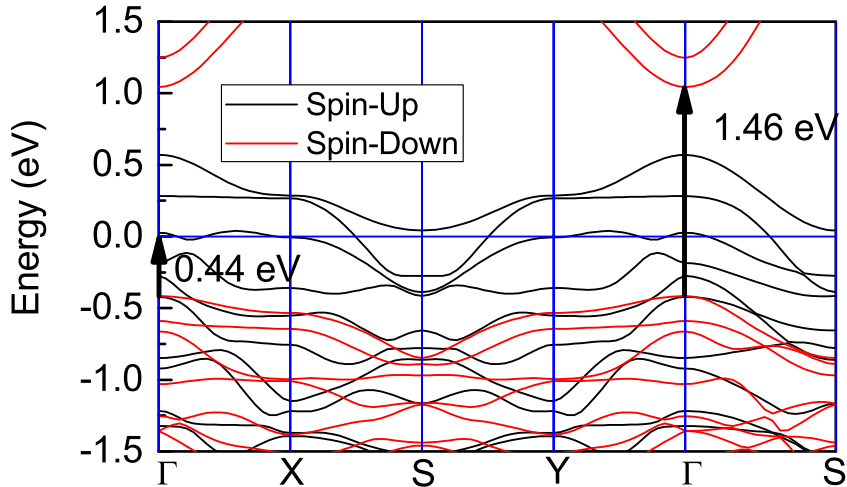


FIG. 2: (Color online) Electronic band structures for single-layer MnAsS₄.

Next, the electronic properties of single-layer MnAsS₄ were investigated. The band structures of single-layer MnAsS₄ are shown in Fig. 2. Notably, the spin-up bands cross the Fermi level, while the spin-down channel acts as a semiconductor, indicating that it is intrinsic half-metallic material with 100% spin-polarization ratio. Comparing with previous studies where half-metallic materials occurred under certain external constraints, the half-metallic material found here is totally intrinsic, meaning that single-layer MnAsS₄ is more suitable for actual spintronic applications. As mentioned before, a wide half-metallic band gap and a wide spin gap are very important for half-metal in spintronic applications^{30,31}. Herein, the half-metallic band gap for single-layer MnAsS₄ is 0.44 eV, which is larger and smaller than the previous research on TiCl₃ (0.42 eV) and on VCl₃ (0.64 eV)¹⁰. The spin gap for the semiconducting channel is 1.46 eV, which is larger than the previous report of Fe₂Si³². The wide spin gap and half-metal gap make 2D MnAsS₄ an ideal candidate for miniaturized spintronic materials. Considering that, approximately 25%-45% of the spin gap is underestimated by DFT method³³, the spin gap of single-layer MnAsS₄ obtained by experiment may be larger than the above value. However, the trends of band dispersions and density of states are qualitatively reasonable, since we are mainly interested in their relative values, and the underestimate should not change the general trends of the results^{34,35}.

Fig. 3 (a) shows the charge density difference of single-layer MnAsS₄. It is the difference between the charge density at the bonding point and the atomic charge density at the

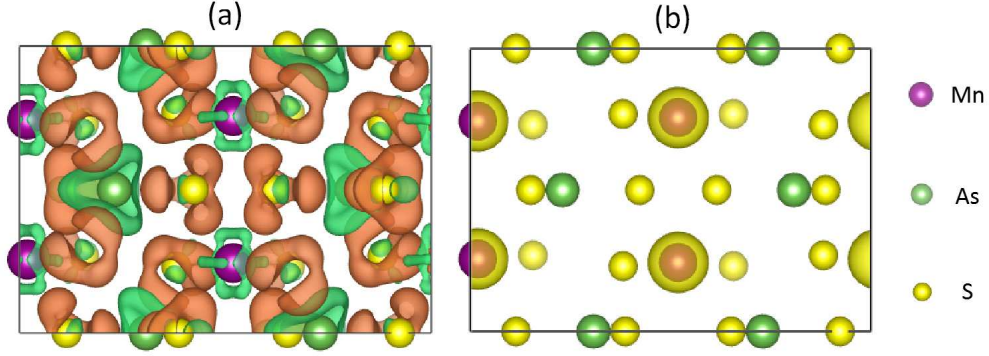


FIG. 3: (Color online) (a) Charge density difference of single-layer MnAsS_4 . The brown (green) region represents the net charge gain (loss). The isosurface value is $0.006 \text{ e}\text{\AA}^{-3}$. (b) Isosurface of spin density with an isovalue of $0.05 \text{ e}\text{\AA}^{-3}$.

corresponding point. The brown and green region represent the charge accumulation and depletion. It is obvious that Mn and As atoms lose electrons and S atoms gain electrons, due to that S atom has larger electronegative. This allows Mn-S bonding to be more ionic. Fig. 3 (b) shows the spin density of single-layer MnAsS_4 , we find that the induced spin polarization is mainly contributed by Mn atoms while the contribution from As and S atoms can be neglected, which is consistent with the magnetic moment analysis.

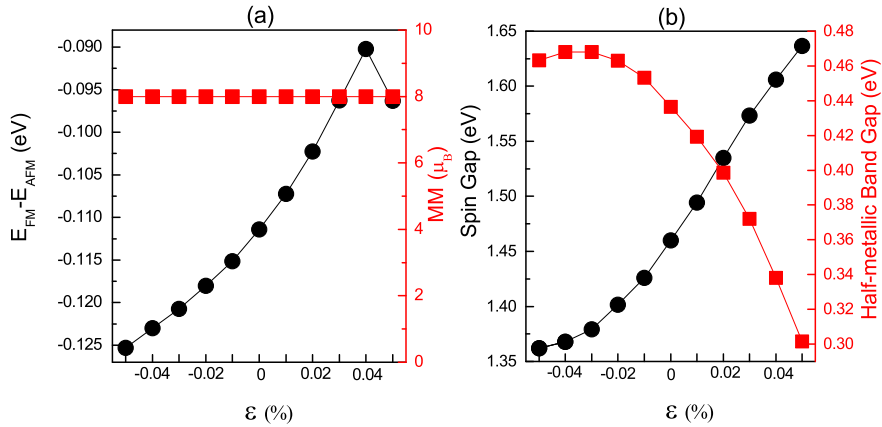


FIG. 4: (Color online) Under biaxial strain for single-layer MnAsS_4 . (a) Energy difference between the FM and AFM phases (black line) and total magnetic moments (red line). (b) Variation of the spin gap (black line) and half-metallic band gap (red line).

Fig. 4 (a) (red line) shows the change of total magnetic moment when a biaxial strain

is applied. We find that the total magnetic moment is not affected when the biaxial strain range from -5% to 5%. Fig. 4 (a) (black line) shows the energy difference between the FM and AFM orderings under the biaxial strain are negative, which indicates that no phase transition occurs during the process of biaxial strain and FM is always ground-state. As shown in Fig. 4 (b) (black line), when the biaxial stretch occurs, the spin gap increases, but decreases when the biaxial compression. When the strain is 5%, the spin gap increases from 1.46 eV to 1.64 eV, and when the strain is -5%, the spin gap decreases to 1.36 eV, this trend is consistent with the previous report of CrSiTe₃³⁶. When applying a biaxial strain of -3%, the half-metallic band gap becomes a maximum of 0.47 eV, but a biaxial stretch decreases the half-metallic band gap. When the biaxial strain is 5%, the half-metallic band gap is 0.30 eV.

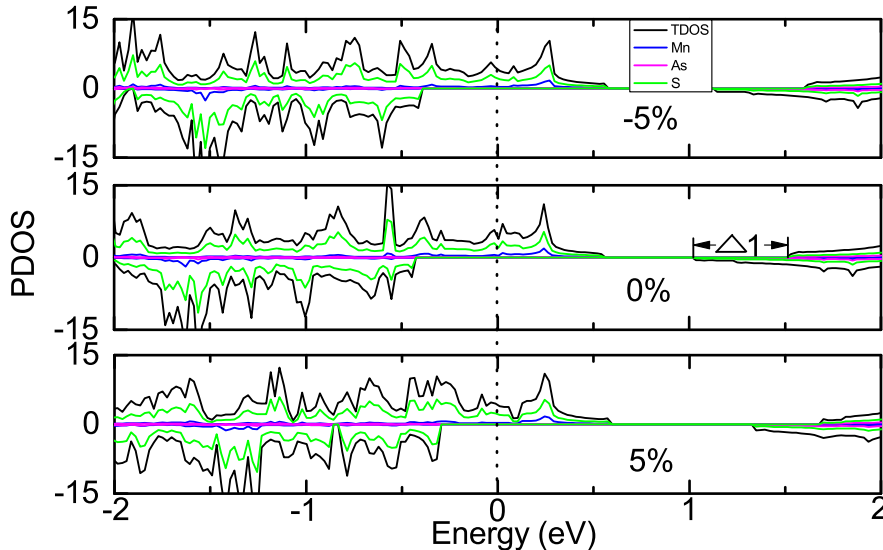


FIG. 5: (Color online) density of states for single-layer MnAsS₄ under different biaxial strain. The percentage in the figure indicates the magnitude of the strain.

For the single-layer MnAsS₄, a large spin exchange splitting of 0.49 eV (labeled as Δ_1 in Fig. 5) in the conduction band is observed, which is crucial for the application in spin-polarized carrier injection and detection³⁷. When applying a biaxial strain of -5% and 5%, spin exchange splitting changes from 0.49 eV to 0.47 eV and 0.35 eV, respectively, which is larger than the CrGeTe₃ (0.24 eV). Whether the strain is compressive or stretching, the density of states all clearly indicates that the contributions near the Fermi energy level come mainly from the electronic state of Mn and S atoms.

To realize spintronic applications for single-layer MnAsS₄, it is necessary to obtain the

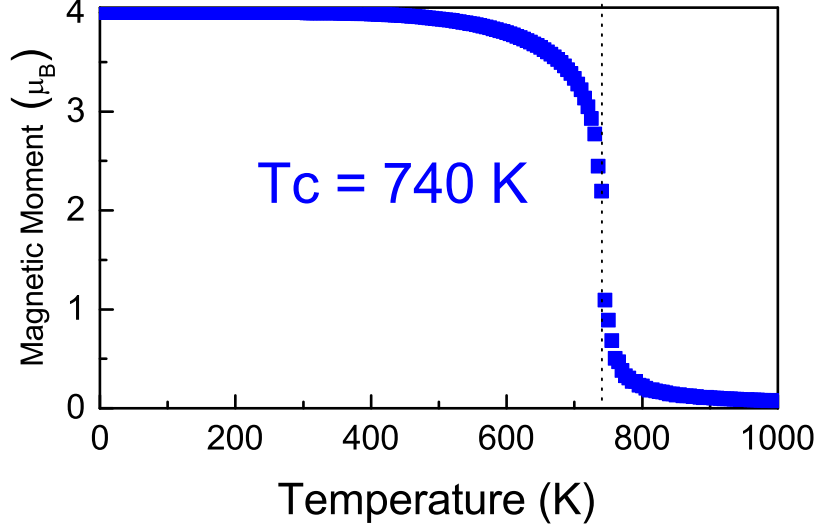


FIG. 6: (Color online) Monte Carlo simulations on the average magnetic moment of Mn atoms for single-layer MnAsS₄ based on Ising model.

variation trend of local magnetic moment with T_c at which MnAsS₄ change from FM state to paramagnetic state. We thus employed Monte Carlo simulations with the Hamiltonian $H = - \sum_{\langle ij \rangle} J_{ij} S_i S_j$ to predicted the FM transition temperature, where J_{ij} represents the exchange interactions of over all neighbor Mn-Mn pairs, S_i represents the spin of atom i . Herein we only consider nearest neighbors located along x and y directions. The exchange interaction parameters J_{ij} are determined by the relation between the total energy and spin configurations. Our result of total J_{ij} is 5.33 meV and 8.71 meV along the x and y directions, respectively, S=2. As shown in Fig. 6, the T_c extracted from the figure is around 740 K. It is significantly higher than those reported before, e.g., CrI₃ monolayer (45 K)³⁸, CrSiTe₃ (35.7 K) and CrGeTe₃ (57.2 K)³⁷

IV. CONCLUSIONS

In summary, we presented a intrinsic ferromagnetic half-metallic material by using first-principles calculations. The calculations of mechanical properties, phonon dispersion and binding energy ensure the stability and the possibility of preparation of single-layer MnAsS₄. The band structures show that the single-layer MnAsS₄ has a 100% spin-polarization ratio at Fermi level. Also, for the semiconducting channel, the spin gap and half-metallic band gap are 1.46 eV and 0.44 eV, respectively. It also has a large spin exchange splitting of

0.49 eV in the conduction band. Within the biaxial strain range from -5% to 5%, the ferromagnetic half-metallic properties remain unchanged. Monte Carlo simulations estimate that T_c for single-layer MnAsS₄ can up to 740 K. The intrinsic half-metallic with high T_c and excellent stability endows single-layer MnAsS₄ a promising functional material for spintronic applications.

V. ACKNOWLEDGMENTS

This work was supported by National Natural Science Foundation of China (No.11904312 and 11904313), the Project of Hebei Educational Department, China(No.ZD2018015 and QN2018012), the Advanced Postdoctoral Programs of Hebei Province (No.B2017003004) and the Natural Science Foundation of Hebei Province (No. A2019203507). Thanks to the High Performance Computing Center of Yanshan University.

REFERENCES

- ¹A. Fert, “Nobel lecture: Origin, development, and future of spintronics,” *Rev. Mod. Phys.* **80**, 1517 (2008).
- ²X. Li and J. Yang, “First-principles design of spintronics materials,” *Natl. Sci. Rev.* **3**, 365 (2016).
- ³Y. P. Feng, L. Shen, M. Yang, A. Wang, M. Zeng, Q. Wu, S. Chintalapati, and C.-R. Chang, “Prospects of spintronics based on 2D materials,” *Wires. Comput. Mol. Sci.* **7**, e1313 (2017).
- ⁴C. Felser, G. H. F. Fecher, and B. Balke, “Spintronics: A challenge for materials science and solid-state chemistry,” *Angew. Chem. Int. Edi.* **46**, 668 (2007).
- ⁵M. Ashton, D. Gluhovic, S. B. Sinnott, J. Guo, D. A. Stewart, and R. G. Hennig, “Two-dimensional intrinsic half-metals with large spin gaps,” *Nano. Lett.* **17**, 5251 (2017).
- ⁶R. A. de Groot, F. M. Mueller, P. G. v. Engen, and K. H. J. Buschow, “New class of materials: Half-metallic ferromagnets,” *Phys. Rev. Lett.* **50**, 2024 (1983).
- ⁷B. Wang, Y. Zhang, L. Ma, Q. Wu, Y. Guo, X. Zhang, and J. Wang, “MnX (P, As) monolayers: a new type of two-dimensional intrinsic room temperature ferromagnetic half-metallic material with large magnetic anisotropy,” *Nanoscale* **11**, 4204 (2019).

- ⁸B. Yang, J. Wang, X. Liu, and M. Zhao, “Promising half-metallicity in ductile NbF₃: a first-principles prediction,” *Phys. Chem. Chem. Phys.* **20**, 4781 (2018).
- ⁹Q. Wu, Y. Zhang, Q. Zhou, J. Wang, and X. C. Zeng, “Transition-metal dihydride monolayers: A new family of two-dimensional ferromagnetic materials with intrinsic room-temperature half-metallicity,” *J. Phys. Chem. Lett.* **9**, 4260 (2018).
- ¹⁰Y. Zhou, H. Lu, X. Zu, and F. Gao, “Evidencing the existence of exciting half-metallicity in two-dimensional TiCl₃ and VCl₃ sheets,” *Sci. Rep.* **6**, 19407 (2016).
- ¹¹H.-H. Xie, R.-Y. Ma, Q. Gao, L. Li, and J.-B. Deng, “Half-metallic ferromagnetism of RbSe and CsTe compounds: A density functional theory study,” *Chem. Phys. Lett.* **661**, 89 (2016).
- ¹²E. Yan, “Half-metallic properties in rocksalt and zinc-blende M N (M = Na, K): A first-principles study,” *Phys. B* **407**, 879 (2012).
- ¹³L. Li, G. Lei, Q. Gao, J.-B. Deng, and X.-R. Hu, “First-principles study on the bulk and (111) surface half-metallicity of KS and RbS in CsCl structure,” *Mater. Res. Bull.* **68**, 308 (2015).
- ¹⁴G. Y. Gao and K. L. Yao, “Half-metallic sp-electron ferromagnets in rocksalt structure: The case of SrC and BaC,” *Appl. Phys. Lett.* **91**, 082512 (2007).
- ¹⁵H. L. Zhuang and J. Zhou, “Density functional theory study of bulk and single-layer magnetic semiconductor CrPS₄,” *Phys. Rev. B* **94**, 195307 (2016).
- ¹⁶P. E. Blöchl, “Projector augmented-wave method,” *Phys. Rev. B* **50**, 17953 (1994).
- ¹⁷G. Kresse and J. Furthmüller, “Efficient iterative schemes for ab initio total-energy calculations using a plane-wave basis set,” *Phys. Rev. B* **54**, 11169 (1996).
- ¹⁸G. Kresse and J. Furthmüller, “Efficiency of ab-initio total energy calculations for metals and semiconductors using a plane-wave basis set,” *Comput. Mater. Sci.* **6**, 15 (1996).
- ¹⁹H. J. Monkhorst and J. D. Pack, “Special points for brillouin-zone integrations,” *Phys. Rev. B* **13**, 5188 (1976).
- ²⁰J. P. Perdew, K. Burke, and M. Ernzerhof, “Generalized gradient approximation made simple,” *Phys. Rev. Lett.* **77**, 3865 (1996).
- ²¹A. I. Liechtenstein, V. I. Anisimov, and J. Zaanen, “Density-functional theory and strong interactions: Orbital ordering in mott-hubbard insulators,” *Phys. Rev. B* **52**, R5467 (1995).

- ²²C. Franchini, R. Podloucky, J. Paier, M. Marsman, and G. Kresse, “Ground-state properties of multivalent manganese oxides: Density functional and hybrid density functional calculations,” *Phys. Rev. B* **75**, 195128 (2007).
- ²³S. L. Dudarev, G. A. Botton, S. Y. Savrasov, C. J. Humphreys, and A. P. Sutton, “Electron-energy-loss spectra and the structural stability of nickel oxide: An LSDA + U study,” *Phys. Rev. B* **57**, 1505 (1998).
- ²⁴A. Togo and I. Tanaka, “First principles phonon calculations in materials science,” *Scr. Mater* **108**, 1 (2015).
- ²⁵T. Hu, W. Wan, Y. Ge, and Y. Liu, “Strain-tunable magnetic order and electronic structure in 2d CrAsS₄,” *J. Magn. Magn. Mater* **497**, 165941 (2020).
- ²⁶Z. Wu, E. Zhao, H. Xiang, X. Hao, X. Liu, and J. Meng, “Crystal structures and elastic properties of superhard IrN₂ and IrN₃ from first principles,” *Phys. Rev. B* **76**, 054115 (2007).
- ²⁷S. Tomar, B. Ghosh, S. Mardanya, P. Rastogi, B. Bhadoria, Y. S. Chauhan, A. Agarwal, and S. Bhowmick, “Intrinsic magnetism in monolayer transition metal trihalides: A comparative study,” *J. Magn. Magn. Mater* **489**, 165384 (2019).
- ²⁸F. Ma, M. Zhou, Y. Jiao, G. Gao, Y. Gu, A. Bilic, Z. Chen, and A. Du, “Single layer bismuth iodide: computational exploration of structural, electrical, mechanical and optical properties,” *Sci. Rep.* **5**, 17558 (2015).
- ²⁹P. Liu, F. Lu, M. Wu, X. Luo, Y. Cheng, X.-W. Wang, W. Wang, W.-H. Wang, H. Liu, and K. Cho, “Electronic structures and band alignments of monolayer metal trihalide semiconductors MX₃,” *J. Mater. Chem. C* **5**, 9066 (2017).
- ³⁰G. Gao, L. Hu, K. Yao, B. Luo, and N. Liu, “Large half-metallic gaps in the quaternary heusler alloys CoFeCrZ (Z = Al, Si, Ga, Ge): A first-principles study,” *J. Alloy. Compd.* **551**, 539 (2013).
- ³¹K.-I. Kobayashi, T. Kimura, H. Sawada, K. Terakura, and Y. Tokura, “Room-temperature magnetoresistance in an oxide material with an ordered double-perovskite structure,” *Nature* **395**, 677 (1998).
- ³²Y. Sun, Z. Zhuo, X. Wu, and J. Yang, “Room-temperature ferromagnetism in two-dimensional Fe₂Si nanosheet with enhanced spin-polarization ratio,” *Nano. Lett.* **17**, 2771 (2017).

- ³³J. P. Perdew, “Density functional theory and the band gap problem,” [Int. J. Quantum Chem. **28**, 497 \(1985\)](#).
- ³⁴Y. Ma, Y. Dai, M. Guo, C. Niu, Y. Zhu, and B. Huang, “Evidence of the existence of magnetism in pristine VX_2 monolayers ($X = S, Se$) and their strain-induced tunable magnetic properties,” [ACS. Nano. **6**, 1695 \(2012\)](#).
- ³⁵M. Joe, H. Lee, M. M. Alyörük, J. Lee, S. Y. Kim, C. Lee, and J. H. Lee, “A comprehensive study of piezomagnetic response in $CrPS_4$ monolayer: mechanical, electronic properties and magnetic ordering under strains,” [J. Phys: Condens. Matter **29**, 405801 \(2017\)](#).
- ³⁶X. Chen, J. Qi, and D. Shi, “Strain-engineering of magnetic coupling in two-dimensional magnetic semiconductor $CrSiTe_3$: Competition of direct exchange interaction and superexchange interaction,” [Phys. Lett. A **379**, 60 \(2015\)](#).
- ³⁷X. Li and J. Yang, “ $CrXTe_3$ ($X = Si, Ge$) nanosheets: two dimensional intrinsic ferromagnetic semiconductors,” [J. Mater. Chem. C **2**, 7071 \(2014\)](#).
- ³⁸B. Huang, G. Clark, E. Navarro-Moratalla, D. R. Klein, R. Cheng, K. L. Seyler, D. Zhong, E. Schmidgall, M. A. McGuire, D. H. Cobden, *et al.*, “Layer-dependent ferromagnetism in a van der waals crystal down to the monolayer limit,” [Nature **546**, 270 \(2017\)](#).